

# A Model of the Tropical Pacific Sea Surface Temperature Climatology

RICHARD SEAGER

*Department of Geological Sciences, Columbia University, New York*

STEPHEN E. ZEBIAK AND MARK A. CANE

*Lamont-Doherty Geological Observatory, Palisades, New York*

A model for the climatological mean sea surface temperature (SST) of the tropical Pacific Ocean is developed. The upper ocean response is computed using a time dependent, linear, reduced gravity model, with the addition of a constant depth frictional surface layer. The full three-dimensional temperature equation and a surface heat flux parameterization that requires specification of only wind speed and total cloud cover are used to evaluate the SST. Specification of atmospheric parameters, such as air temperature and humidity, over which the ocean has direct influence is avoided. The model simulates the major features of the observed tropical Pacific SST. The seasonal evolution of these features is generally captured by the model. Analysis of the results demonstrates the control the ocean has over the surface heat flux from ocean to atmosphere and the crucial role that dynamics play in determining the mean SST in the equatorial Pacific. The sensitivity of the model to perturbations in the surface heat flux, cloud cover specification, diffusivity, and mixed layer depth is discussed.

## 1. INTRODUCTION

Sea surface temperature (SST) is a critical parameter for many problems of atmosphere-ocean interaction in tropical and equatorial regions. The ascending nodes of planetary scale thermally forced circulation cells are related not only to intense surface heating over tropical land masses but also to the warmest SSTs (e.g., the equatorial west Pacific). Descending air is found at higher latitudes and over cooler ocean waters (e.g., the equatorial east Pacific). It is clear that if coupled atmosphere-ocean models are to successfully simulate planetary scale circulation features, then the large-scale pattern of the tropical SST field must also be simulated.

Predicting SST is potentially more difficult in the tropics than in mid-latitudes because although surface heat flux is often still dominant, vertical and horizontal advections of heat can be very important. Further, the currents are driven by the winds, which themselves are related to the SST distribution. This coupling between atmosphere and ocean is enhanced because the surface heat flux across the ocean surface is influenced by such atmospheric parameters as clouds, wind speed, air temperature, and humidity, all of which are related to both the atmospheric dynamics and the SST.

Coupling an ocean model with an atmosphere general circulation model (GCM) would allow direct computation of the radiative flux at the sea surface. In addition, the parameters required to estimate the latent and sensible heat fluxes, using the standard bulk formulae, could be computed. In the absence of an atmospheric GCM the atmospheric parameters can be taken from data and the radiative fluxes also computed from bulk formulae using cloud cover data. This was the approach of Han [1984]. Han (following Haney [1971]) wrote his heat flux parameterization in the form

$$Q = D(T_A - T_s) \quad (1)$$

$T_A$  is an "apparent" equilibrium temperature, and  $D$  is a heat transfer coefficient; both are computed by a linearization of the full bulk formulae around the local air temperature.  $D$  and  $T_A$  vary both temporally and spatially. Han used this formulation with a six-layer primitive equation world ocean model to produce a tropical SST field that bears an impressive similarity to the observed field. Meehl *et al.* [1982] used a formulation like (1) in their global ocean general circulation model but chose the simplest form by assuming that  $D$  is a constant and  $T_A$  equals the air temperature. They do not present maps of SST, and consequently the successes and failures of the SST simulation cannot be assessed. Philander and Pacanowski (1986a, b) in a primitive equation model of the tropical Atlantic Ocean assumed constant solar radiation equatorward of 20° latitude and constant long-wave back radiation, and they used standard bulk formulae to compute the latent and sensible heat flux. They assumed a constant relative humidity of 80%, used observed air temperature in the sensible heat flux formula, and assumed a minimum wind speed of 4.8 m s<sup>-1</sup>. This latter assumption is intended to account for evaporation by high-frequency winds not present in the mean monthly winds used for driving the model. Since they do not present maps of SST, it is not possible to evaluate the success of this aspect of the simulation.

In this paper we consider the problem of developing an ocean model that includes a surface heat flux parameterization that is both capable of being coupled to a simple atmosphere model [e.g., Zebiak, 1982, 1986] and excludes the specification of parameters over which the ocean has direct influence (such as near-surface temperature and humidity). The atmospheric parameters that can be included in such a model are wind speed, saturation humidity (a function of SST alone), and cloud cover. Cloud cover is included on the assumption that it can be specified simply or related to some large-scale feature of the atmospheric circulation. Because both sensible heat flux and net long-wave radiation depend on air temperature, and this cannot justifiably be specified externally, these two terms of the surface heat flux must be represented in terms of the SST. Here we exploit the observation that over most of the

Copyright 1988 by the American Geophysical Union.

Paper number 7C0794.  
0148-0227/88/007C-0794\$05.00

ocean, the air temperature closely parallels the SST. Further, we avoid the requirement to know the atmospheric humidity by specifying a constant relative humidity. Computing the heat flux in this manner imposes limitations, but it is considered worthwhile to see how successfully SST can be simulated in the absence of an atmospheric GCM or extensive application of data. The heat flux parameterization has the virtue of being independent of atmospheric parameters such as air temperature and humidity that are difficult to predict with accuracy.

We demonstrate that it is possible to simulate the major features of the climatological mean SST in the tropical Pacific using the heat flux parameterization presented here. This result suggests that once the solar flux is given, the remainder of the surface heat flux is controlled by the ocean. The results encouraged us to attempt to identify the underlying processes that determine tropical SST. Section 2 of the paper will describe the model, section 3 will be a general comparison of model and observed SSTs, section 4 will consider the sensitivity of the model to parameter changes, and section 5 will address the seasonal cycle of temperature and the balance of terms in the temperature equation for key regions of the tropical Pacific. Conclusions are presented in section 6.

## 2. MODEL DESCRIPTION

### 2.1. Dynamical Model

The dynamical model is that of *Zebiak and Cane* [1987] but modified to simulate total rather than anomaly SSTs. The basin is rectangular extending from 124°E to 80°W and from 29.75°S to 29.75°N. The model describes the linear dynamics of an homogeneous upper layer, overlying a motionless deep layer, on an equatorial beta plane, subject to a low-frequency approximation. A constant depth, frictional, linear surface layer is included above this layer to capture the intensity of wind driven surface currents. The equations for the second and surface layer combined can be written as

$$\partial u/\partial t - \beta_0 y v = -g' \partial h/\partial x + \tau^x/\rho H - ru \quad (2)$$

$$\beta_0 y u = -g' \partial h/\partial y + \tau^y/\rho H - rv \quad (3)$$

$$\partial h/\partial t + H(\partial u/\partial x + \partial v/\partial y) = -rh \quad (4)$$

where

$$\mathbf{u} = (H_1 \mathbf{u}_1 + H_2 \mathbf{u}_2)/H \quad (5)$$

Here,  $\mathbf{u}_1$  and  $\mathbf{u}_2$  are the velocities in the surface layer and second layer, respectively,  $H_1$  is the depth of the surface layer, and  $H_2$  is the mean depth of the second layer.  $H$  is the mean depth of the dynamically active fluid and  $h$  represents anomalies in this depth. Otherwise, the notation follows standard conventions.

The equations for the surface Ekman flow,  $\mathbf{u}_s = \mathbf{u}_1 - \mathbf{u}_2$ , are

$$r_s u_s - \beta_0 y v_s = \tau^x/\rho H_1 \quad (6)$$

$$r_s v_s + \beta_0 y u_s = \tau^y/\rho H_1 \quad (7)$$

$\mathbf{u}_1$  is determined from equations (2)–(7) and can be used to calculate the entrainment velocity (which equals the upwelling velocity for a constant depth mixed layer) from

$$w_s = H_1(\partial u_1/\partial x + \partial v_1/\partial y) \quad (8)$$

The surface layer temperature  $T_s$  is then computed from

$$\begin{aligned} \partial T_s/\partial t + u_1 \partial T_s/\partial x + v_1 \partial T_s/\partial y + M(w_s)\gamma(T_s - T_d)/H_1 \\ = Q/\rho c_p H_1 + \nu(\partial^2 T_s/\partial x^2 + \partial^2 T_s/\partial y^2) \end{aligned} \quad (9)$$

$T_d$  is the temperature immediately beneath the base of the surface layer,  $M(w_s)$  is defined to be zero for  $w_s$  less than zero and to equal  $w_s$  for  $w_s$  greater than or equal to zero, and  $\gamma$  is such that the temperature of entrained water,  $T_e$ , is given by

$$T_e = (1 - \gamma)T_s + \gamma T_d$$

$\gamma$  is taken to be 0.75. Other parameter values are  $H = 150$  m,  $H_1 = 50$  m,  $g'H = 2.9$  m s<sup>-1</sup>,  $r = 2.5$  year<sup>-1</sup>, and  $r_s = 2$  day<sup>-1</sup>.

The numerical procedure for solution of (2)–(5) is given by *Cane and Patton* [1984]. Briefly, the Kelvin wave part of the solution is solved for analytically, and the remainder is solved by finite difference method on a staggered grid exploiting the fact that this part of the solution propagates westward only. Solving in this manner and using the low-frequency approximation, allows a 10-day time step on a grid with spacing of 2° longitude and 0.5° latitude. The boundary conditions for the system are no normal flow at the basin boundaries. Equations (6) and (7) for the surface layer are two algebraic equations in two variables that are trivial to solve. Equation (9) is solved by forward time differencing evaluating the advection terms with a modified upwind difference scheme as described by *Zebiak* [1984]. The grid spacing is 2° in latitude and 5.625° in longitude, allowing a time step of 2.5 days. The boundary conditions at the eastern and western edges are no normal advection and temporally varying climatological temperatures from *Rasmusson and Carpenter* [1982] are imposed at 29°N and 29°S. Because the Ekman flow described by (6) and (7) is poleward at these latitudes, the climatological temperatures affect the computation only through the diffusion term. We present results only for the near-equatorial latitude range of interest, 20°S to 20°N, well away from this influence. The component of diffusion normal to the eastern and western boundaries is set to zero; that is, there is no heat flux through these walls.

### 2.2. Determination of the Temperature of Entrained Water ( $T_e$ )

The most straightforward procedure is to represent the temperature beneath the base of the surface layer ( $T_d$ ) by the temperature at 50-m depth ( $T_{50}$ ). The problem then becomes predicting  $T_{50}$  in terms of the other model variables. We assume that temperature perturbations are coherent with depth below the turbulent mixed layer. Thus  $T_{50}$  can be parameterized in terms of vertical displacements of the model thermocline (i.e., the variable  $h$  in (2)–(4)). This formulation has the property that where the thermocline is shallow (e.g., the equatorial east Pacific), upwelled water originates from the thermocline region and is cold. On the other hand, where the thermocline is deep (e.g., the equatorial west Pacific), upwelled water originates from above the thermocline and is warm. This is only qualitatively correct because upwelling may occur from variable depths.

To represent this process in the model, a relationship was developed between  $T_{50}$  and the thermocline depth from data, and a second relationship was derived between model  $h$  and the observed thermocline depth. The data set of *Levitus*

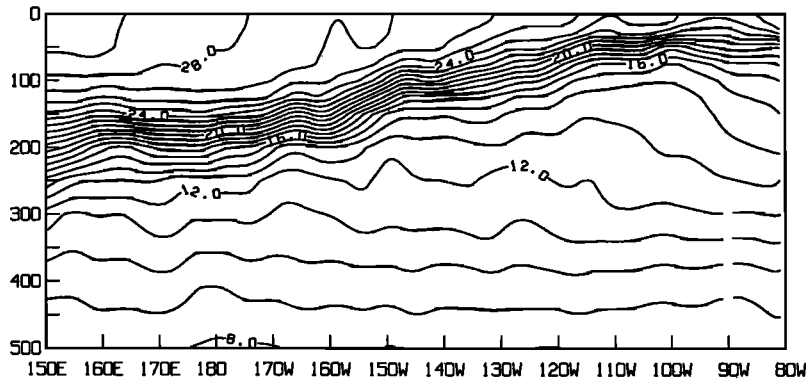


Fig. 1. Equatorial cross section of temperature for May, June, and July [after Levitus, 1982].

[1982] was used to obtain temperature as a function of depth for the global ocean and four seasons. Because upwelling, and hence  $T_d$  in equation (9), will be important only in equatorial regions (and some coastal regions) only data from 4.5°N to 4.5°S in the Pacific Ocean were analyzed. As a proxy for thermocline depth the depth of the 20°C ( $h_{20}$ ) isotherm was used, which is a reasonable approximation in this latitude range (see Figure 1). Figure 2 shows the scatter of points for all seasons on a plot of  $T_{50}$  against  $h_{20}$ . The line is a best fit curve derived using a cubic spline with six “knots” chosen to be concentrated in the region where the scatter of points indicates the most curvature. The line has a least squares error in temperature of 0.73°C. The curve is modified by the conditions that  $T_{50}$  never exceed 29.8°C and that for  $h_{20}$  less than 26 m  $T_{50}$  is set equal to 17.1°C. This latter condition avoids a slight but undesired increase of  $T_{50}$  with decreasing  $h_{20}$  in the range of  $h_{20}$  greater than zero but less than 26 m.

For the next step the model was run with the climatological monthly winds of Rasmusson and Carpenter [1982] and values of model thermocline depth anomaly,  $h$ , stored once the model was spun up. Values for the latitude range 4.5°S to 4.5°N were extracted and a regression performed to produce the relation

$$h_{20} = b_0 + b_1 h + b_2 h^2 \tag{10}$$

which has a correlation coefficient of 0.969. The scatter of values for  $h$  and  $h_{20}$  and the curve described by (10) are shown in Figure 3.

A quadratic fit was chosen for the following reasons. In nature the easterly momentum equation on the equator, for small friction, is given by

$$\rho g' h_{20} \partial h_{20} / \partial x = \tau^x$$

where  $h_{20}$  is understood to represent the depth of the thermocline. However, in the linear model the balance is instead

$$\rho g' H \partial h / \partial x = \tau^x$$

Setting the stresses equal to each other and integrating gives

$$h_{20}^2 = 2Hh + c$$

where  $c$  is some constant. It follows that

$$h_{20} = c^{1/2} (1 + Hh/c - H^2 h^2 / 2c^2 + \dots)$$

Simple theory then predicts a polynomial relationship between the observed thermocline depth and its model analogue. We choose to use only the first three terms in the expansion.

With these two relations, for each value of  $h$  computed, a value of  $T_d$ , which equals  $T_{50}$  as derived from the cubic spline

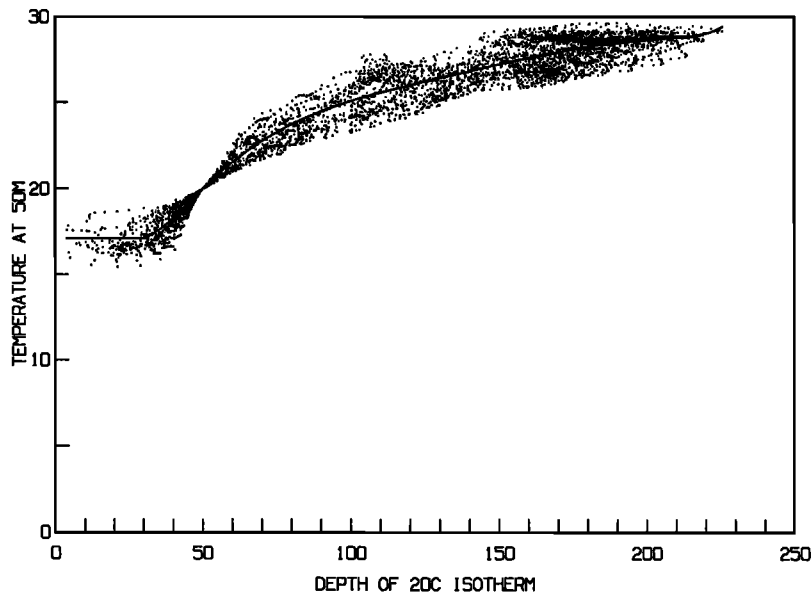


Fig. 2. Temperature at 50-m depth as a function of depth of the 20°C isotherm with best fit curve derived by cubic spline method. Data are from Levitus [1982].

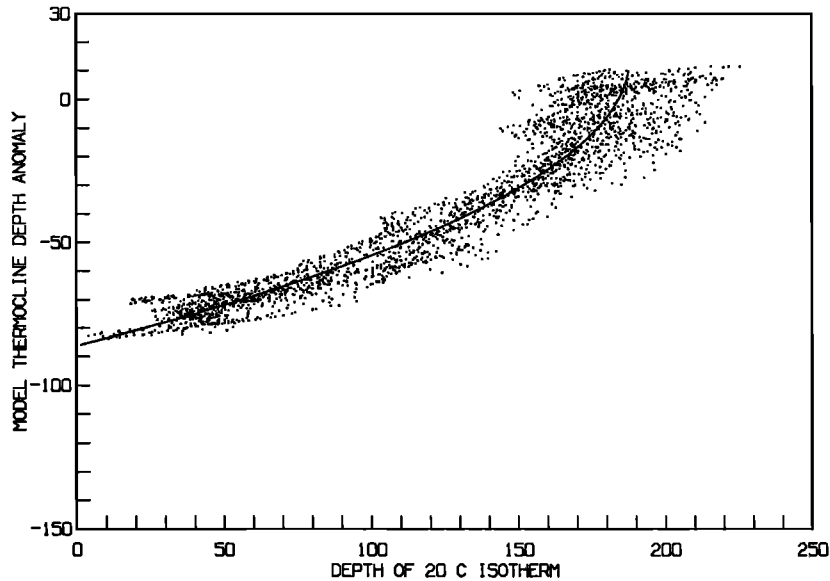


Fig. 3. Model thermocline depth anomaly as a function of depth of 20°C isotherm with best fit curve derived by second-order linear regression. The regression coefficient equals 0.969.

in Figure 2, can be calculated and used in (9). Because upwelling, and hence vertical advection, are important only in the near-equatorial region and along the South American coast, outside of the region between 5°N and 5°S at all longitudes and extending to 15°S for the area east of 96°W,  $T_d$  is set equal to the surface temperature less 0.5°C. Experiments with different treatments of the off-equatorial  $T_d$  have shown the nature of this formulation to have trivial or zero influence on the SST field.

### 2.3. Surface Heat Flux Parameterization

First we will discuss why it was decided to compute the surface heat flux, rather than use observed values. Figure 4 shows the annual mean surface heat flux of Weare *et al.* [1980], and Figure 5 shows that of Esbensen and Kushnir [1981]. Both are computed using bulk formulae with ship reports of meteorological variables and surface temperature as input data. If nothing else, the two maps make clear that there is considerable uncertainty regarding the pattern and magnitude of the surface heat flux (cf. Talley, 1984). For example, Weare *et al.*'s data show a prominent maximum in downward heat flux over the equatorial west Pacific which is absent in Esbensen and Kushnir's data. The differences are partly attributable to use of different bulk formulae. Another difference is that Weare *et al.* compute a heat flux for each ship report and then average the fluxes in time and space, whereas Esben-

sen and Kushnir compute time- and space-averaged fluxes from averaged measured variables. The cumulated differences are large, and ocean model runs using these heat fluxes would produce very different SSTs.

According to Weare *et al.* [1981], the 95% confidence interval for net annual surface heating is  $\pm 49 \text{ W m}^{-2}$ , corresponding to a standard deviation of  $25 \text{ W m}^{-2}$ , when the error is introduced by sampling biases. Blanc [1987] estimated that in addition, the error introduced into latent heat flux estimates by measurement error and the calibration of bulk formulae was greater than 40%. A difference of  $25 \text{ W m}^{-2}$  can change the temperature of 50 m of water by over  $3.5^\circ\text{C yr}^{-1}$ , a level of error that would be intolerable in an ocean model integration. What is more, if the model was run with imposed heat flux, it would have to come into equilibrium with that heat flux. This would mean that using Weare *et al.*'s data would result in an SST that was excessively warm in the equatorial west Pacific, since no presently acting ocean process could balance that quantity of heating. Elsewhere, errors of over  $4^\circ\text{C}$  would occur that were due to nothing more than errors in the surface heat flux. Uncertainties in the heat flux data would dominate the results to such an extent that little else could be learned. We are forced to conclude that specifying the heat flux from data would introduce a degree of uncertainty that would obscure the results of the ocean model. It was decided to compute the heat flux from a modified version of the usual bulk formulae.

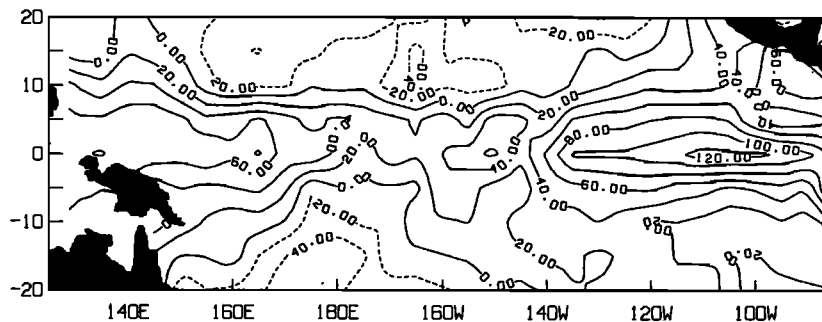


Fig. 4. Annual mean downward surface heat flux according to Weare *et al.* [1980].

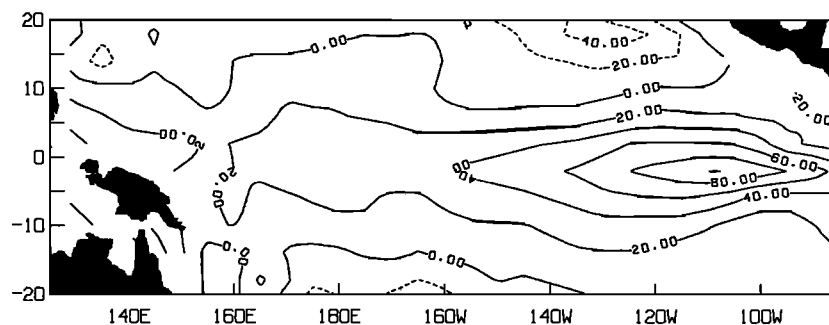


Fig. 5. Annual mean downward surface heat flux according to *Esbensen and Kushnir* [1981].

As was discussed in the introduction, we will include only those parameters that can realistically be considered as externally imposed, that is, those over which the ocean has no direct control. These are wind speed and total cloud cover, with air temperature and humidity excluded. The thesis here is that the air temperature is determined by the SST, not the other way around. To include it in a heat flux parameterization is to include a constraint on the SST tantamount to putting in a large part of the answer.

The solar flux is computed according to the formula given by *Weare et al.* [1980]. This computes the solar radiation at the surface under clear skies ( $Q_0$ ) according to a harmonic formula that introduces variability with latitude and time of year. This is then corrected for cloud cover  $C$ , noon solar altitude  $\theta$ , and surface albedo  $A$ . The latent heat flux is computed from the standard bulk formula using a fixed humidity factor  $\delta$  and exchange coefficient  $C_E$ . A minimum wind speed is imposed, for this term only, which acts as a parameterization for evaporation by high-frequency winds excluded in the monthly winds. A further heat loss term, proportional to  $T_s$  (in degrees Celsius), is included and is designed to represent the sensible and long wave radiative heat losses. The atlas of *Weare et al.* [1980] indicates these two terms to be considerably smaller than the solar and latent heat terms in the heat budget and to have a variability over the tropical Pacific of less than  $20 \text{ W m}^{-2}$  combined.

With these assumptions the net surface heat flux is given by

$$Q = (1 - A)(1 - 0.62C + 0.0019\theta)Q_0 - \rho_a C_E L |v|(1 - \delta)q_s - \alpha(T_s - T^*)$$

The first term on the right is the solar heating, the second term is the latent heat loss, and the final term is the representation of the net long wave radiation and sensible heat loss. The saturation humidity  $q_s$  is evaluated from the Clausius-Clapeyron equation using the surface temperature  $T_s$ . Since the humidity factor multiplies the saturation humidity evaluated at the surface temperature, it is related to the relative humidity ( $\delta_{rh}$ ), expressed as a fraction, by

$$\delta = \delta_{rh} q_s(T_s) / q_s(T_a)$$

where  $T_a$  is the surface air temperature.

We take the surface albedo to be 0.06, a value typical of the tropical oceans [*Payne*, 1972];  $\alpha$  is assumed equal to  $1.5 \text{ W m}^{-2} \text{ K}^{-1}$ .  $T^*$  is taken as 273.15 such that, rather arbitrarily, this term is proportional to the SST in degrees Celsius. It provides an upward heat flux in the range  $30\text{--}45 \text{ W m}^{-2}$ , which according to the data of *Weare et al.* [1980] approximates the observed basin mean flux of sensible heat and long-

wave radiation combined.  $C_E$  is assumed to be a constant  $1.5 \times 10^{-3}$ .

### 3. MODEL RESULTS FOR THE STANDARD CASE

For the standard case we assume  $\delta = 0.70$ , which for a SST of  $25^\circ\text{C}$  typically corresponds to a relative humidity of 72–73%, a minimum wind speed of  $4 \text{ m s}^{-1}$ , a diffusivity of  $2 \times 10^4 \text{ m}^2 \text{ s}^{-1}$ , and spatially varying but annually averaged cloud cover as given by *Weare et al.* [1980]. The model was run for 10 years, starting from rest and a uniform temperature of  $25^\circ\text{C}$ , using the monthly climatological winds of *Rasmusson and Carpenter* [1982]. The model is fully spun up after 7 years, and all the results we present are from year 10 of the run.

Figures 6a and 6b present simulated SSTs for January and July, and Figures 7a and 7b present differences relative to the observed SSTs of *Rasmusson and Carpenter* [1982] for the seasons December, January, and February (DJF) and June, July, and August (JJA). For the purpose of display only, these fields have been smoothed by application of a (1-2-1) in  $x$  and  $y$ . The differences seen involve an overestimation of the temperature in the warmest areas, such as the equatorial west Pacific and off the coast of Mexico, and underestimation of the temperature in the region  $10^\circ\text{--}20^\circ\text{N}$  and  $130^\circ\text{E}$  to  $140^\circ\text{W}$ . The error can reach up to  $3^\circ\text{C}$  but the root-mean-square temperature error is only of the order of  $1^\circ\text{C}$ . In addition there is a seasonally varying error off what would be the South American coast, this area being too cold in DJF and too warm in JJA. Outside of this area, and the region of the North Equatorial Countercurrent (NECC), the errors are remarkably constant with season. This is seen in Figures 8 and Figures 9a and 9b, which show the annual mean differences and the differences for DJF and JJA after the annual mean error has been removed. The root-mean-square error in the seasonal temperature variation is less than  $0.5^\circ\text{C}$  but it is over  $1^\circ\text{C}$  for the annual mean. Only the area off the coast of South America has an error in the seasonal cycle that is large.

The major elements of the seasonal development of the SST field are represented. In the following we will provide a description and attempt to explain their origin. The southeastern section is characterized by water getting colder eastward toward the coast and southward to higher latitudes. This cold patch extends into the equatorial cold tongue. The tongue is weakest in northern hemisphere (NH) spring when this entire southeastern area is at its warmest. The opposite situation holds in NH fall. This cycle is followed by both model and observations although the model is phase lagged by one month. To the south of the equator the annual cycle can be related, in both cases, to the cycle of surface heating forced by

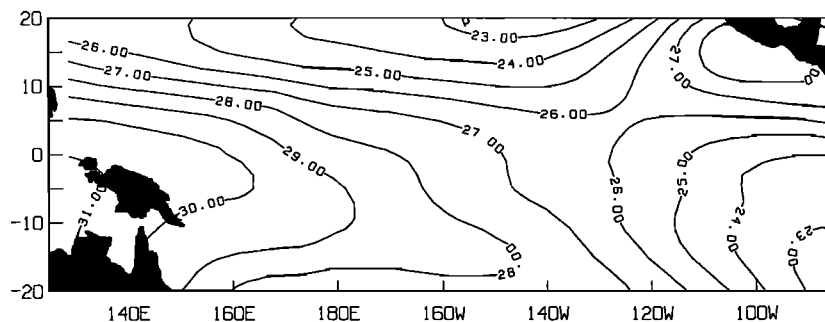


Fig. 6a

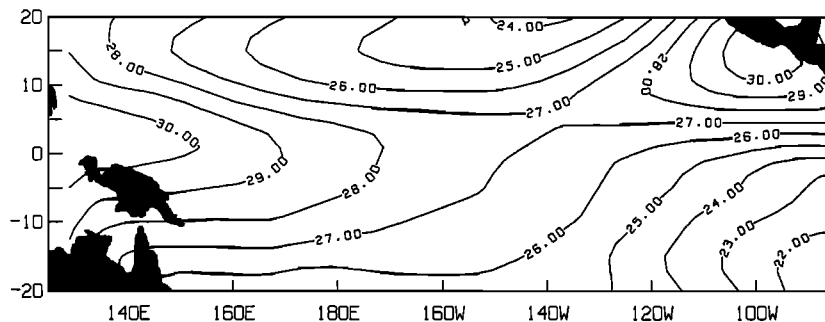


Fig. 6b

Fig. 6. Simulated sea surface temperature in the standard run for (a) January and (b) July.

variations in the solar flux. The coldness of the region in the annual mean, in our model, is primarily due not to coastal upwelling or advection of cold water from the south, but to a maximum of cloud cover which induces a minimum of surface heating, relative to areas to the north and west.

For the equatorial cold tongue the maximum SST in NH spring is related to a combination of weak cooling due to upwelling (because of weak zonal winds along the equator and a deep thermocline) and strong surface heating. During NH fall, when the SST is a minimum, there is strong cooling due to upwelling (because the zonal winds along the equator are strong and the thermocline is shallow) which overpowers the surface heating. The model indicates that zonal and meridional advection aid the cooling but have significant effects only when the tongue is most developed. The seasonal cycle will be discussed in more detail in section 5.

The west Pacific warm pool is easily explained as an area where the surface heat flux is either near zero or downward throughout the year. Upwelling, meridional advection, and diffusion all do little here, so the region becomes warm with surface heat flux balanced primarily by changes in SST and zonal advection. The downward heat flux is the result of a minimum in upward latent heat flux related to a wind speed minimum typical of areas of atmospheric convergence. Since in our model this region is too warm, it is worth considering the problems that would have been incurred if we had used the surface heat flux of *Weare et al.* [1980] (Figure 4) with its very large maximum of downward heat flux over the equatorial west Pacific. Another local minimum of wind speed, together with the limited influence of dynamics, is responsible for the second warm spot off the coast of Mexico. The south-eastward extension of the west Pacific warm pool is also relat-

ed to a minimum of wind speed associated with the South Pacific convergence zone (SPCZ).

The warm strip which joins these two warm regions has a nebulous origin. In our model it does not owe its existence to advection of warm water from the west Pacific warm pool even though it is in the region of the North Equatorial Countercurrent. Zonal velocities and temperature gradients are not large enough for that to be the case. It is more easily explained as a region of surface heat gain sandwiched between a region of cooling due to upwelling to the south, and an area of strong latent heat loss to the northwest under the core of the trades. It will be considered in more detail in section 6.

At higher latitudes the SST is determined by a one-dimensional balance of heat storage in the mixed layer and surface heat flux, resulting in a simple annual cycle of temperature. In both the NH and southern hemisphere (SH) strong cooling by latent heat loss occurs in the central parts of the ocean during NH summer and fall. This is the time when the northeast trades are their strongest and the SPCZ its weakest. In the NH this results in the development, in the model, of a tongue of cold water following the core of the trades. The western end of this tongue is responsible for preventing the observed northward migration of the west Pacific warm pool during NH summer. The tongue is not observed in nature. In the SH the cooling is responsible for destroying the south-eastward extension of the west Pacific warm pool which observations indicate is still present, although weakened, in this season. It is plausible that in these areas the cloud cover is less than is indicated by the surface data.

Differences between model and observed SSTs near the coast of South America and off the coast of Mexico can, in part, be attributed to failings in the parameterization of the

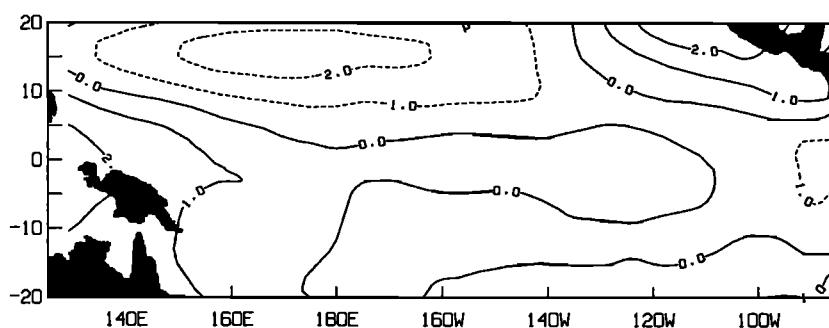


Fig. 7a

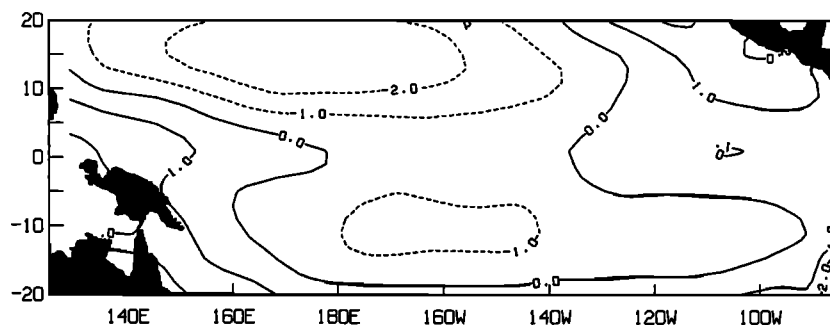


Fig. 7b

Fig. 7. Simulated minus observed sea surface temperature in the standard run for (a) DJF and (b) JJA.

temperature of entrained water, or absence of baroclinic surface boundary currents in the simulation. For example, the model does not simulate the northward flowing Peru Current along the South American coast. The advective cooling thus neglected would be strongest in NH fall, when the current is strong and the temperature gradient along the coast a maximum. In agreement with this observation the model is too warm here during this season. Cloud cover is also greatest at this time, but a run using monthly rather than annual cloud cover did not cool this area significantly.

Differences over the warmest waters in the west Pacific are difficult to attribute with certainty to any particular model deficiency but could easily be due to errors in the cloud correction parameterization, the minimum wind speed assumption in the latent heat loss formula, or a humidity factor that is below the assumed 0.70. Less likely, it could be due to underestimation of horizontal advection. This is also the case in the northeastern region of the basin, where the model is consistently too cold, and once again, the problem is most likely to lie in the surface heat flux. It should be noted that changes in the cloud cover by 30% or less are sufficient to remove all the differences between the model and observed SSTs, except in the extreme southeast corner. While this does not necessarily imply that the cloud cover data are incorrect, it does indicate that errors of a reasonable magnitude in the atmospheric parameters are sufficient to account for discrepancies between the model and the observed SSTs of the magnitude seen here. This is not a claim that the model is correct, but a statement that its faults cannot be detected by looking at SST alone.

The preceding discussion raises the question of the relative effects of surface heat flux and ocean dynamics in determining the SST. To illustrate this, a model run was performed in

which there was no dynamics and no diffusion. In this case the SST at each point was determined by the surface heat flux alone. Meehl and Washington [1985] performed this experiment using a 50-m-depth mixed layer and a surface heat budget determined by the National Center for Atmospheric Research (NCAR) community climate model. Figures 10a and 10b show SSTs for January and July produced by our model, while model minus observed SSTs for the seasons DJF and JJA are shown in Figure 11a and 11b. The most striking change is that the equator is now an SST maximum at all longitudes. In addition, the warm spot off the coast of Mexico has become excessively hot, and the cold region in the northwest of the model ocean has cooled off by another degree. The results are similar to those of Meehl and Washington [1985] except that they have a further region of model temperatures colder than observed at 10°–20°S to the west of 110°W, and a cold region off the coast of Central America. The similarity of the two experiments is, however, more qualitative than quantitative. It should be noted that differences between the results presented here and those of Meehl and Washington [1985] are due solely to the contrasting treatment of the heat flux and that the discrepancies are once again in the annual mean and not in the seasonal cycle. This comparison displays the extent to which treatment of the surface heat flux can influence the SST. In addition, the importance of dynamics in the tropical heat budget is clearly demonstrated: without them not a single prominent feature of the tropical SST field remains intact.

#### 4. SENSITIVITY STUDIES AND OTHER CASES

A number of experiments were performed to analyze the sensitivity of the model to changes in the heat flux parameterization, cloud cover, and diffusion.

To assist in understanding the results of these experiments,

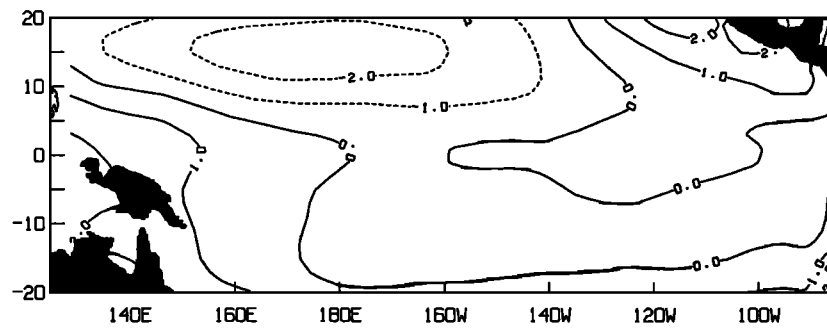


Fig. 8. Simulated minus observed annual mean sea surface temperature in the standard run.

two preliminary runs were performed, one with a constant addition of  $10 \text{ W m}^{-2}$  into the ocean everywhere and one with a constant extraction of  $10 \text{ W m}^{-2}$  everywhere. A local estimate of the partial derivative  $\partial T_s / \partial Q$  is computed from the difference in SST between the two runs. This is of interest since it includes not only feedbacks in the surface heat flux but also the effects of the dynamics; that is, it provides an estimate of the temperature change that results from a given change in the surface heat flux after adjustments due to changes in the surface heat flux and redistribution by currents and diffusion.

The annual mean estimate of  $\partial T_s / \partial Q$  is shown in Figure 12. There is a large minimum centered in the region of maximum equatorial upwelling. In this area the dynamics are highly active, and perturbations in the surface heat flux are, to a large extent, overwhelmed by advective effects. The other major features are two maxima over the warmest waters, one in the equatorial west Pacific and the other off the coast of Mexico. These are regions of minimum wind speed and less active dynamics, which first prohibits a large negative feedback in

the surface heat flux and second prevents the distribution of the imposed heat flux change over a large area. As a result, the SST is most sensitive to changes in the surface heat flux in these two regions. In the regions of low sensitivity a heat flux perturbation of  $25 \text{ W m}^{-2}$  is required to change the SST by  $1^\circ\text{C}$ , but in regions of high sensitivity this SST change can be accomplished by a perturbation of only  $12 \text{ W m}^{-2}$ . These sensitivities can easily be transferred into relaxation times for a mixed layer with depth of 50 m. The smallest value of  $\partial T_s / \partial Q$  (0.04) then corresponds to a relaxation time of 93 days, and the largest value (0.08) corresponds to 186 days. This provides an indication of the time scale for persistence of the effects of surface heat flux perturbations.

The following experiments were performed: (1) a decrease of the humidity factor to 0.68, (2) a decrease of the minimum wind speed in the heat flux parameterization to  $3.5 \text{ m s}^{-1}$ , (3) replacement of annually averaged cloud cover with monthly varying cloud cover, (4) replacement of annually averaged cloud cover with constant cloud cover of 58% everywhere,

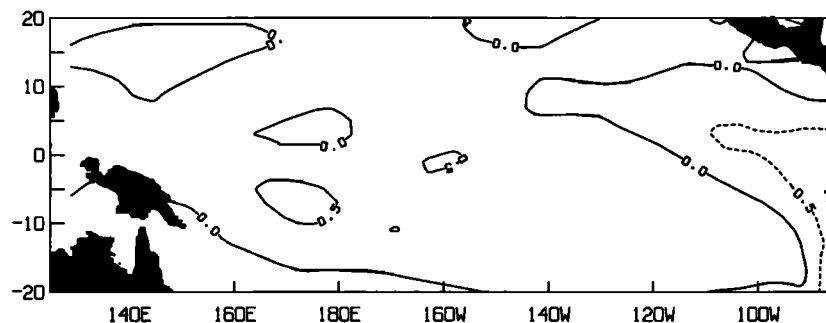


Fig. 9a

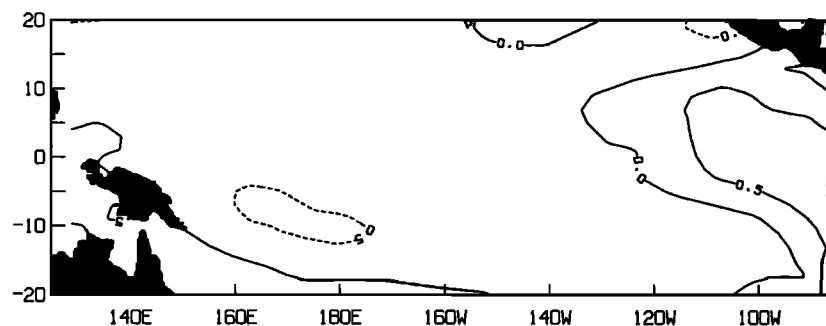


Fig. 9b

Fig. 9. Simulated minus observed sea surface temperature with annual mean difference removed for (a) the standard run and DJF and (b) the standard run and JJA.

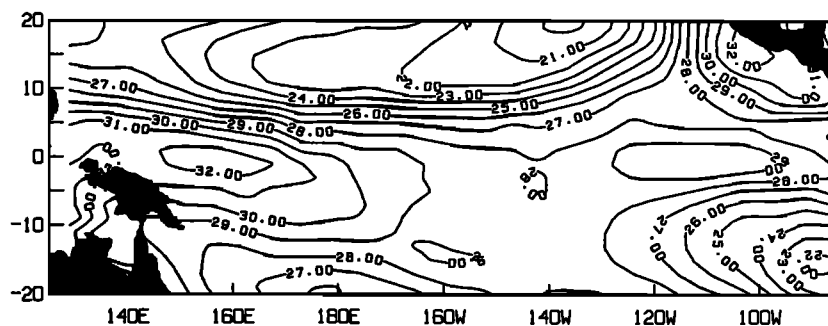


Fig. 10a

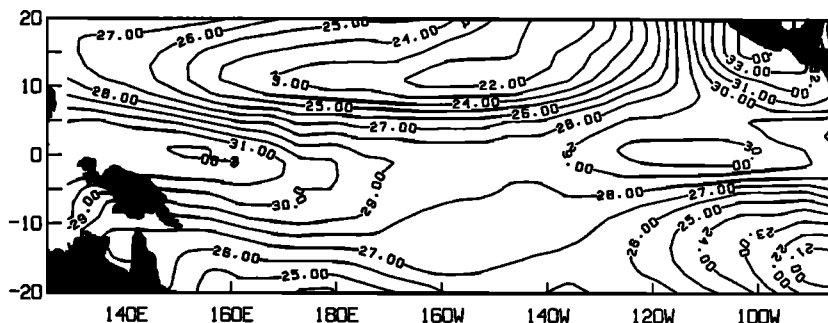


Fig. 10b

Fig. 10. Same as Figures 6a and 6b but for case with no dynamics and no diffusion.

and (5) a 1 order of magnitude decrease in diffusivity to  $2 \times 10^3 \text{ m}^2 \text{ s}^{-1}$ . In the interest of brevity we present results for JJA only. These are shown in Figures 13a–13e, which should be compared to Figure 7b for the standard case. Figure 13a shows the case for a 0.02 reduction in the humidity factor, which amounts to an approximately 7% reduction in the latent heat flux. The model cools everywhere by typically  $1^\circ\text{C}$  except over the region of maximum equatorial upwelling, where the change is noticeably less than  $1^\circ\text{C}$ . The change is about  $1^\circ\text{C}$  in both the equatorial west Pacific and off the coast of Mexico, where although the latent heat flux is low, the sensitivity is high, and also in the core of the trades, where although the sensitivity is low, the latent heat flux is large. Increasing the humidity factor to 0.72 resulted in a temperature change that is roughly the negative of that produced by case 1.

Figure 13b shows the case for a reduction of the minimum wind speed from  $4 \text{ m s}^{-1}$  to  $3.5 \text{ m s}^{-1}$  which initially reduces the upward heat flux in regions with wind speed of less than  $3.5 \text{ m s}^{-1}$  by 12.5%. The effect is almost entirely confined to these regions and is seen as an increase of temperature by no more than  $1^\circ\text{C}$ . Increasing the minimum to  $4.5 \text{ m s}^{-1}$  produced a similar change in the opposite direction. In both this and case 1 the changes are overwhelmingly in the annual mean, with the seasonal cycle little affected.

The next two runs involved changes in the specified cloud cover. First we replaced the annual mean cloud cover with the monthly varying cloud cover as given by *Weare et al.* [1980]. The differences between this run and the standard case are a little larger in other seasons than in JJA, but it is striking how little of the errors we have seen so far are the result of ignoring seasonally varying cloud cover. (Compare Figures 13c and 7b.) Figure 13d shows the result when the cloud cover is a constant

58% everywhere, a figure which corresponds to a basin mean cloud cover. The differences are much larger than in the previous case, and the SST produced is significantly worse than in the standard case. The errors are what would be expected from a consideration of the observed cloud cover, with the model becoming much too warm in regions of high cloud cover (e.g., the west Pacific) and far too cold in regions of low cloud cover (e.g., the core of the trade winds). Taken together with the previous case, this run demonstrates the extent to which the effect on the SST of time-varying clouds is of secondary importance compared with the effect of the annual mean cloud cover distribution. This also supports the assertion in the previous section that the cold water in the southeast section of the basin is partially caused by a local maximum of cloud cover which reduces surface heating. In this constant cloud cover case this area becomes much warmer.

Figure 13e shows the JJA temperature differences for the case of a 1 order of magnitude decrease in the diffusion coefficient. Clearly, the pattern of differences is the same as in the standard case but accentuated, especially in the regions of high temperature gradient. However, over most of the basin the difference with respect to the standard case is less than  $1^\circ\text{C}$ , indicating that diffusion is of sizeable significance only in those regions, such as to the north of the cold tongue, where the dynamics and surface heating set up large gradients of temperature. In an interesting study, *Hansen and Paul* [1984] used data from satellite-tracked buoys to demonstrate the existence of eddies in the equatorial east Pacific just north of the equator. They attributed these to barotropic instability of the velocity shear between the South Equatorial Current and the NECC. Observations supported a down gradient eddy heat flux dominated by the meridional component. The heat flux

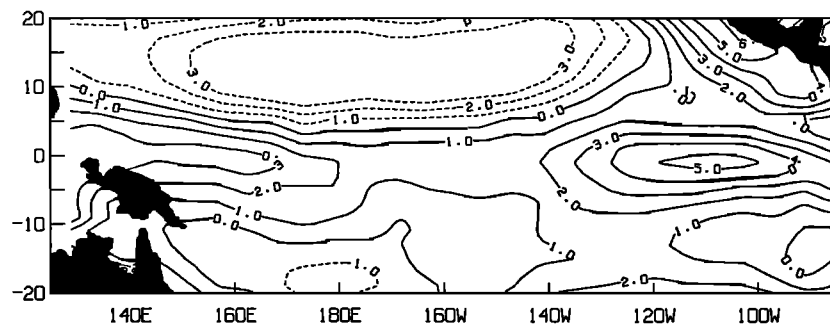


Fig. 11a

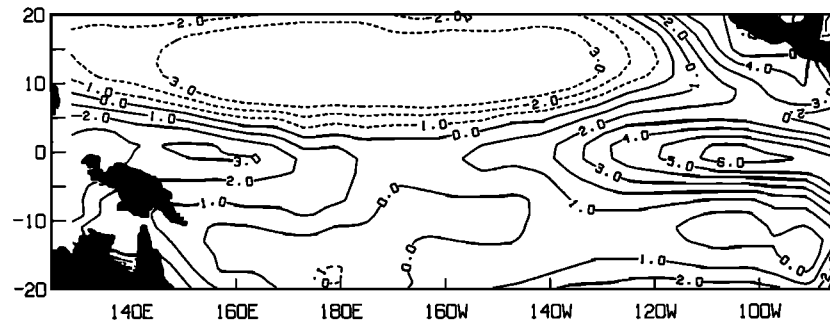


Fig. 11b

Fig. 11. Same as Figures 7a and 7b but for case with no dynamics and no diffusion.

could be reasonably characterized by an eddy diffusivity of  $4 \times 10^4 \text{ m}^2 \text{ s}^{-1}$ , which is twice the value used in the standard case presented here.

One further experiment (not shown) was performed. The mixed layer depth  $H_1$  was reduced to 40 m and the  $T_d$  parameterization reformulated accordingly. The SST produced was nearly indistinguishable from that produced in the standard case. Overall, the basin warmed by  $0.2^\circ\text{C}$ , for two reasons. First, vertical advection, associated with equatorial upwelling, was reduced because  $T_d$  increases. Second, because over most of the ocean the surface heat flux is downward, the shallower surface layer results in a warmer SST. In the higher northern latitudes, where the surface heat flux is upward for most of the year, the moderate cooling tendency contributed by the shallower surface layer is offset by increased meridional advection from the slightly warmer equatorial regions to the south. We concluded that the model does not exhibit significant sensitivity to changes in the surface layer depth in the region of interest, but we would not expect this to be the case in higher latitudes.

##### 5. ANALYSIS OF THE SEASONAL CYCLE OF TEMPERATURE AND HEAT BALANCE

In this section the seasonal cycle of temperature for three different ocean regions is considered, and the role the individual terms in the temperature equation play in determining this variation is analyzed. The three regions correspond to the equatorial cold tongue, an off-equatorial area in the southern hemisphere, and the region of SST maximum north of the cold tongue in the east Pacific which coincides roughly with the region of the North Equatorial Countercurrent. The model parameter settings are those of the standard case described in section 3.

##### 5.1. The Equatorial Cold Tongue

This area extends from  $99^\circ\text{W}$  to  $129^\circ\text{W}$  and  $4^\circ\text{S}$  to  $4^\circ\text{N}$ . Figure 14a shows the cycle of observed and simulated temperature, and Figure 14b shows the cycle of the terms in the temperature equation averaged over this region. The observed SST is tracked fairly well, but the model is phase lagged by 1 month. For example, during NH spring, a time when the tongue is its least developed and the thermocline is deep, the model is too cold. According to the data of Levitus [1982], the thermocline depth is near 80 m but, using (10), the model thermocline depth is nearer 70 m. This leads to an underestimate of  $T_d$  and an overestimate of cooling due to upwelling. These thermocline depths fall in the range where  $T_d$  is very sensitive to changes in the thermocline depth. The assumption of a constant humidity factor contributes to this error. The data of Weare *et al.* [1980] indicate this region to be a local maximum of relative humidity.

Figure 14b demonstrates that in this region all the terms in the temperature equation are important, but that the largest terms contributing to the temperature tendency are the surface heat flux and upwelling advection. Zonal advection, meridional advection, and diffusion, the former two cooling terms and the latter a warming term, have a cycle of strength closely tied to the seasonal development of the tongue itself. This makes sense in that the tongue is produced by upwelling and that the upwelling strength is proportional to the horizontal divergence of velocity: the stronger the currents the stronger the upwelling. Further, when the upwelling is strong, the temperature gradients imposed are large, allowing the possibility of sizeable advection of heat by horizontal currents. Similarly, diffusion increases as the cold tongue develops and creates a marked temperature minimum on the equator.

The balance between surface heat flux, zonal advection and

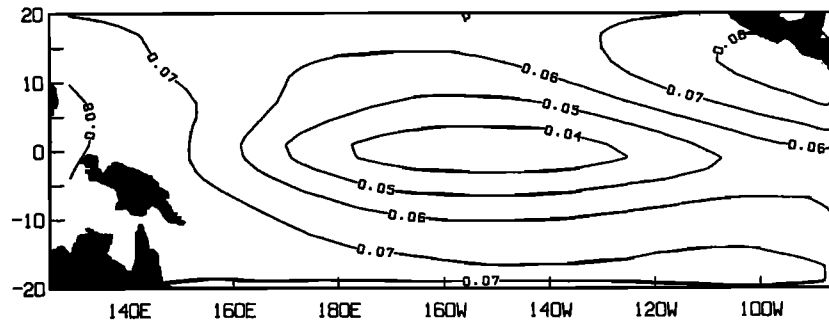


Fig. 12. Estimate of the annual mean value of  $\partial T_s/\partial Q$  in the standard run (in kelvins per watt per square meter).

upwelling advection suggested by Wyrski [1981] for the cold tongue is not seen in our model. Wyrski notes that an eddy diffusivity of the order of  $10^4 \text{ m}^2 \text{ s}^{-1}$  would be required to make diffusion significant. As was discussed in section 4, there is observational evidence for using a diffusivity that large.

The seasonal cycle can be explained as follows. During NH spring the intertropical convergence zone (ITCZ) is at its southernmost position and the zonal winds on the equator are at their weakest resulting in a minimum in upwelling strength. This position is reversed in NH fall, when the ITCZ is well to the north and there are strong zonal winds along the equator. At this time, upwelling is strongest and the tongue most pronounced. This enhancement is aided by the thermocline's being at its shallowest in the east at this time, a phenomenon forced by the contemporaneous maximum of zonal wind stress integrated along the equator. All these processes are represented in the model.

### 5.2. Higher-Latitude Region

This region extends from  $161^\circ\text{W}$  to  $131^\circ\text{W}$  and  $18^\circ\text{S}$  to  $10^\circ\text{S}$ . It is of interest because of the different dynamical regime, the seasonal cycle of surface heat flux, and its location under the eastern extremity of the SPCZ. Figure 15a shows the seasonal cycle of temperature, and Figure 15b shows the seasonal cycle of the components of the temperature equation. The seasonal cycle is simulated with phase close to that observed but can be close to  $1^\circ\text{C}$  too cold in SH winter and spring. From Figure 15b it is seen that the heat balance is essentially between change of heat content and the surface heat flux, which reduces (9) to

$$\partial T_s/\partial t = Q/\rho c_p H_1$$

It should be remembered that we assume a constant depth mixed layer in the model, but according to the data of Levitus [1982], in this region the layer depth varies from typically 50 m around March to 80–100 m around September. The discrepancies in mixed layer depth between model and observations are of the sign to explain the errors. In SH winter the mixed layer is deeper than 50 m, so that for a given upward heat flux, the model would cool more than is observed. The error is prevented from being worse only by the feedback between surface heat flux and SST: as the SST cools the upward heat flux decreases to reduce further cooling.

At the same longitudes and latitudes in the northern hemisphere, although the annual mean is off by a larger amount, the seasonal cycle is also simulated well and for similar reasons. At these latitudes a simple one-dimensional, variable depth mixed layer will accurately simulate SST.

### 5.3. North Equatorial Countercurrent Region

This region extends from  $145^\circ\text{W}$  to  $115^\circ\text{W}$  and  $4^\circ\text{N}$  to  $12^\circ\text{N}$ . It is of oceanographic interest in that it includes the longitudes and latitudes of the NECC and is of meteorological interest because it underlies the eastern Pacific portion of the ITCZ. As is shown in Figure 16a, the simulated seasonal cycle of temperature has the observed amplitude but is phase shifted relative to that observed by about 3 to 4 months. It might be considered that this discrepancy is due to an error in the representation of the NECC itself resulting in errors in the zonal advection. However, the model's zonal velocity field (not shown) shows the NECC to have the correct seasonal cycle, being strongest in NH summer and fall. In accordance with observations, it does not extend farther north than  $10^\circ\text{N}$ . Figure 16b indicates that zonal advection is a minor term in the heat balance in this region, and further consideration of the model's zonal advection field demonstrated that at no time is there significant warming associated with the NECC.

In our model the temperature cycle of this region is determined primarily by the surface heat flux and to a lesser extent by diffusive heat loss. Meridional advection is a heat source during the early half of the year, when the strip of warm water is in the southern part of the area, and is a heat sink in the later half of the year, when the strip is to the north and cold water is advected in from the cold tongue. Interestingly, the data of Weare *et al.* [1980] indicate that the time of maximum observed temperature in the region (April to June) lags the time of maximum downward surface heat flux by 1 month. This maximum is related to a maximum in incoming solar radiation. The model surface heat flux also peaks around the time of maximum SST, but this does not occur until August. It should be noted that in the model, the existence of this strip of warm water is related not to any geographical maximum of downward surface heat flux, but to its position between the region of equatorial upwelling and the region of strong latent heat loss at  $10^\circ\text{N}$  to  $15^\circ\text{N}$  west of  $130^\circ\text{W}$ .

It should be remembered that the equatorial cold tongue also reached its highest temperatures too late, but by 1 month rather than 3. Nonetheless, an area too cold to the south will cause an overestimation of cooling by meridional advection in the warm strip to the north. This would not seem to be of the magnitude required to explain the erroneous phase. Using monthly cloud cover also did not introduce a noticeable improvement. One final point is that an imposed cycle of additional surface heat flux, with maximum in NH spring, minimum in NH fall, and amplitude of less than  $20 \text{ W m}^{-2}$  would be sufficient to remove the discrepancy.

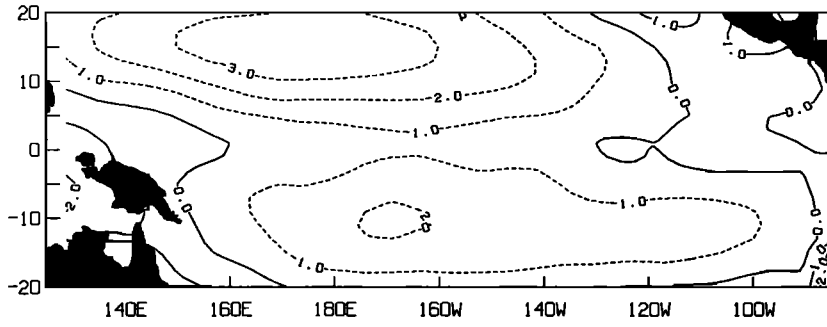


Fig. 13a

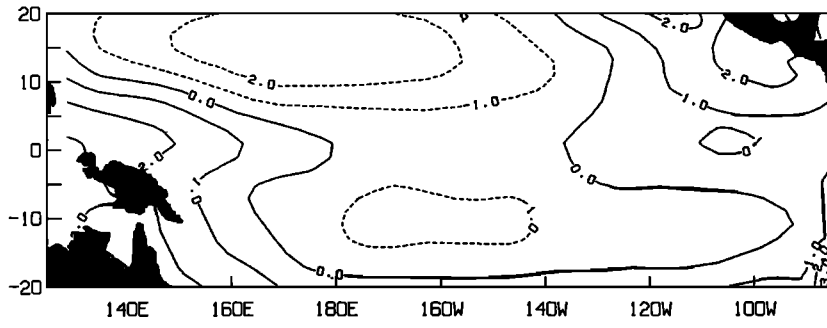


Fig. 13b

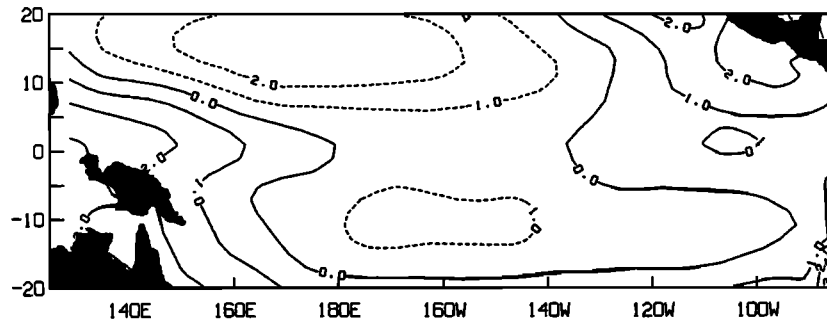


Fig. 13c

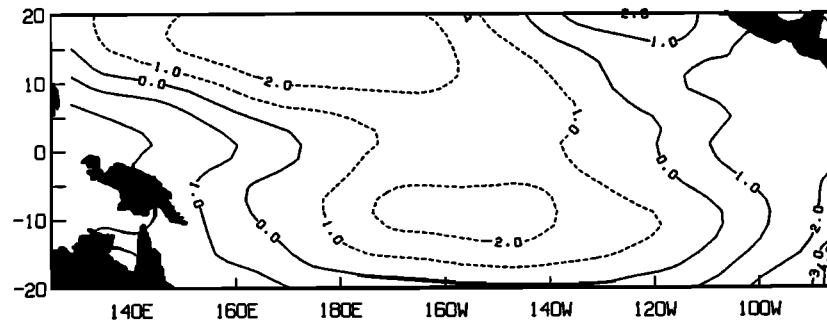


Fig. 13d

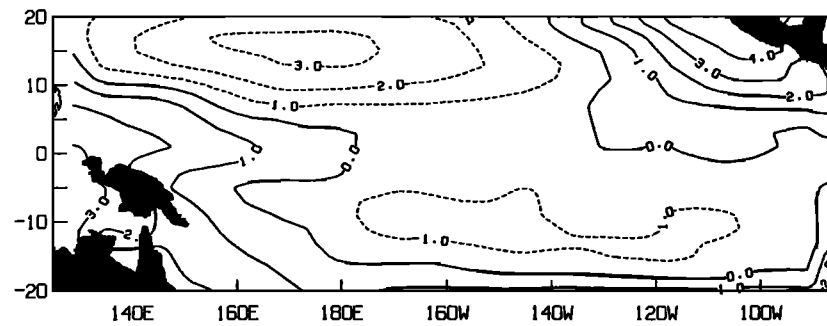


Fig. 13e

Fig. 13. Same as Figure 7 but for (a) humidity factor of 0.68, (b) minimum wind speed of  $3.5 \text{ m s}^{-1}$ , (c) monthly mean cloud cover, (d) constant cloud cover of 58% everywhere, and (e) diffusion coefficient of  $2 \times 10^3 \text{ m}^2 \text{ s}^{-1}$ , all for JJA only.

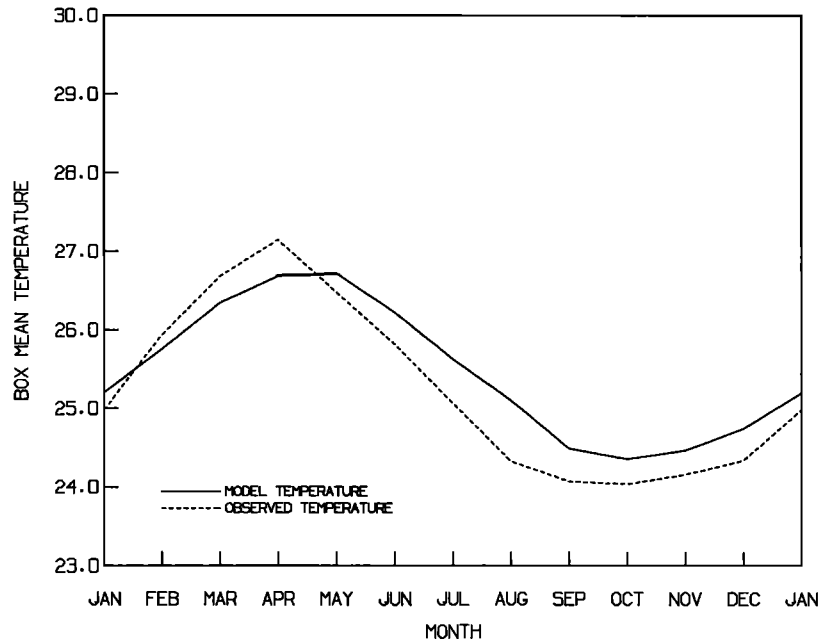


Fig. 14a

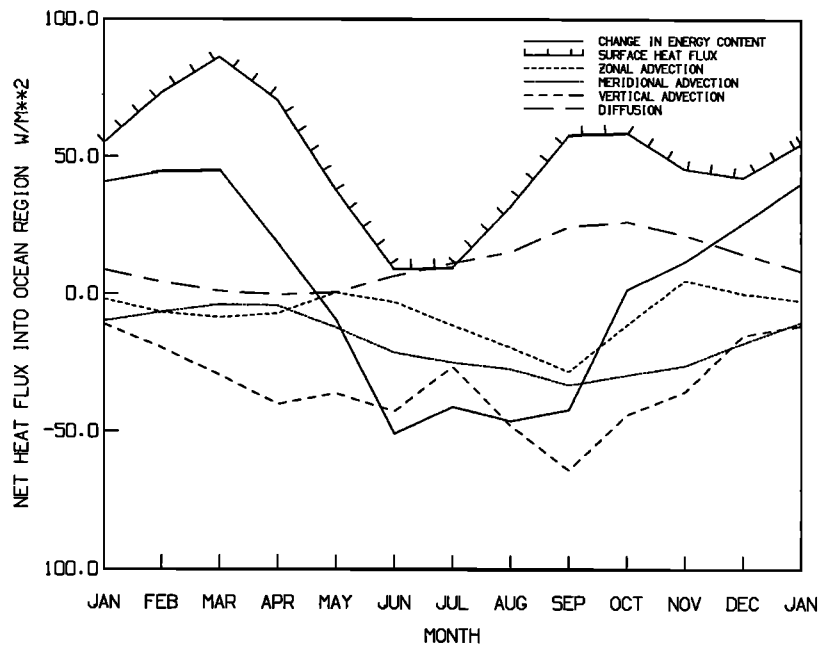


Fig. 14b

Fig. 14. Seasonal cycle of (a) simulated and observed sea surface temperature and (b) components of the temperature equation for the standard run in the region from 129°W to 99°W and 4°S to 4°N.

## 6. DISCUSSION AND CONCLUSIONS

An ocean model has been presented that is capable of simulating most of the features of the mean tropical Pacific SST field. The model requires only winds and annual mean cloud cover as external inputs. Both of these can legitimately be considered to be parameters over which the ocean has at most indirect control. Other parameters, such as humidity and near-surface air temperature, are largely controlled by the ocean, and so we do not wish to specify them in the heat flux parameterization when the goal is to compute SST. In avoiding the specification of these variables, we obtain two advantages. First, the model can be coupled to simple atmosphere models which do not predict these variables, and second, the model is not sensitive to the expected errors in the determi-

nation of these variables with more complex atmosphere models (e.g., GCMs). This second advantage is especially valuable given the strength of the feedbacks which can amplify small, persistent errors.

It is encouraging that this success has been achieved through the application of linear dynamics in a shallow water model. The indication is that the fundamental dynamic processes that determine SST are captured within the linear approximation. However, fully nonlinear thermodynamics are required to simulate the SST. This simple model is also proving relevant in current runs simulating interannual variability and bodes well for future coupled atmosphere-ocean runs.

The major discrepancies in the simulation of SST are the overestimation of the temperatures of the warmest waters (equatorial west Pacific and off the coast of Mexico) and the

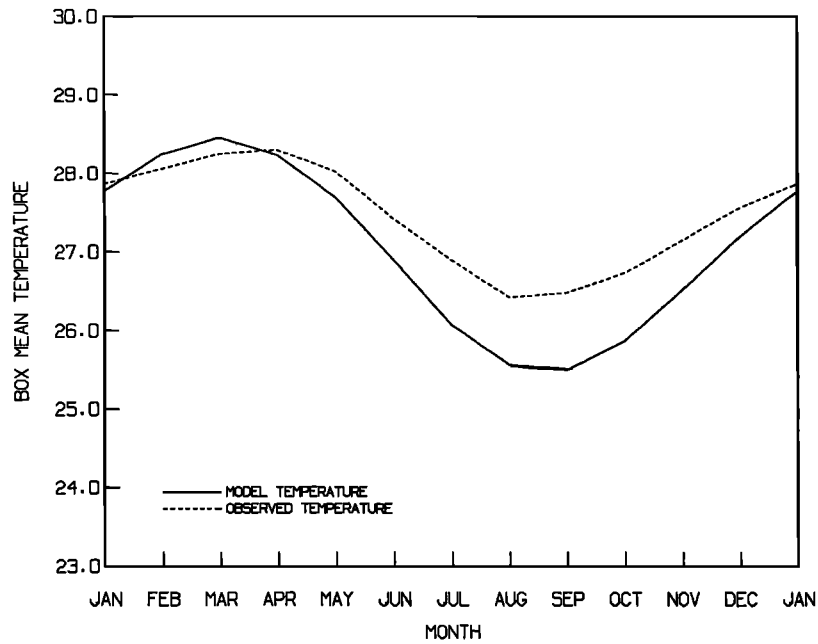


Fig. 15a

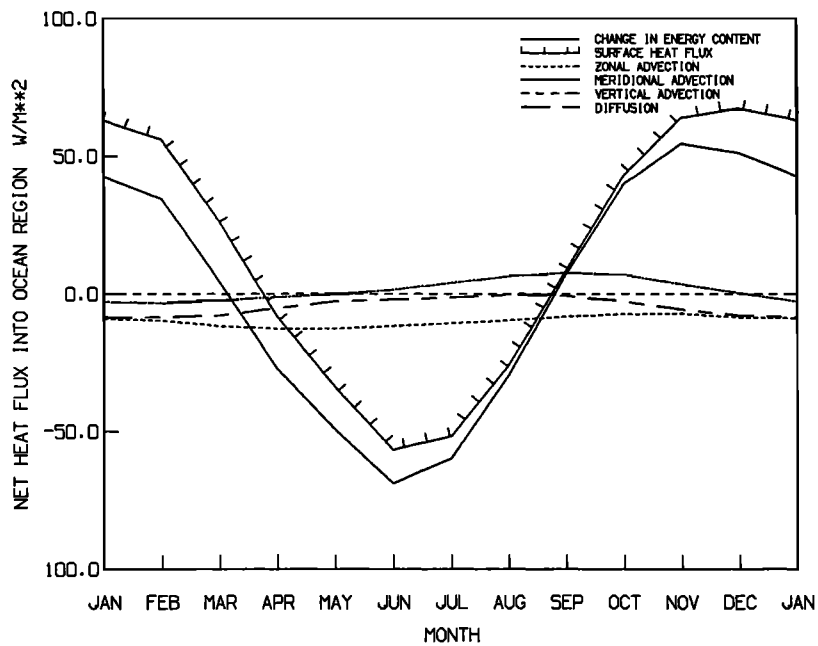


Fig. 15b

Fig. 15. Same as Figure 14 but for the region from 131°W to 161°W and 18°S to 10°N.

underestimation of the temperature under the northeast trades and the SPCZ. It has been pointed out that these are annual mean errors and that the seasonal errors are smaller. In these regions, ocean dynamics contribute only moderately to the temperature tendency, and hence it is reasonable to suspect that the surface heat flux causes the discrepancies. For example, the sensitivity of the SST to small changes in the relative humidity has been shown.

The cloud cover data used in the model are derived from surface observations. These are frequently considered to be unreliable, but at present, no satellite derived data set of sufficient length is available for the purposes required here. It was noted that changes in observed cloud cover of typically 30% or less are sufficient to remove the discrepancies between observed and model SSTs. In this light it should be remembered

that the unit for cloud cover reporting corresponds to 12.5%. A 30% change is required off the coast of Mexico and in the center of the northeastern cold patch. Changes of greater than 30% would be required in the extreme southeast corner, where there are obviously problems other than those related to the surface heat flux.

The cloud cover data derived from the International Satellite Cloud Climatology Program (ISCCP) for July 1983, the only month available at the time of writing, are interesting in this respect. Total cloud cover is lower than that indicated by climatological surface observations over the northeastern cold patch and in the area between the SPCZ and the equatorial cold tongue, whereas it is higher off the coast of Mexico and over the west Pacific. Preliminary results of the ISCCP analysis include a tropical cloud cover that has more spatial varia-

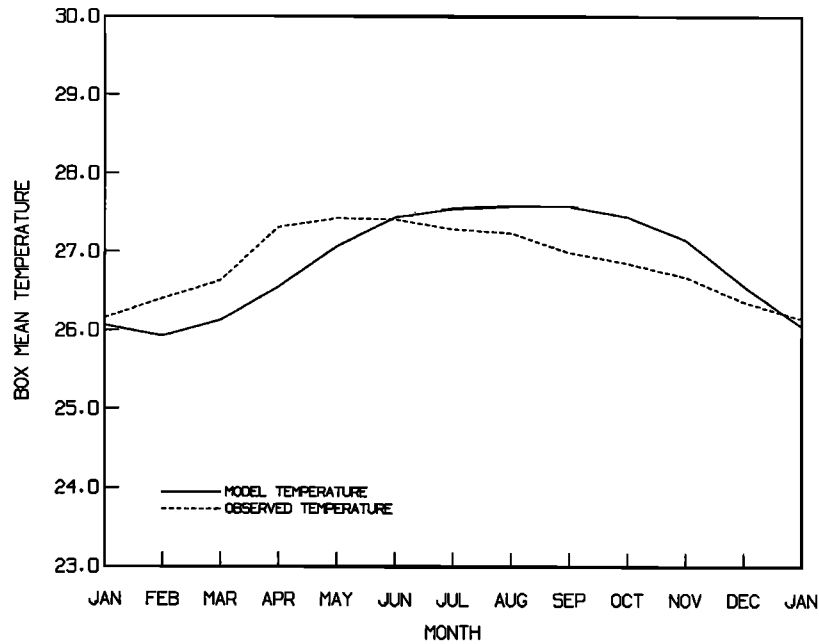


Fig. 16a

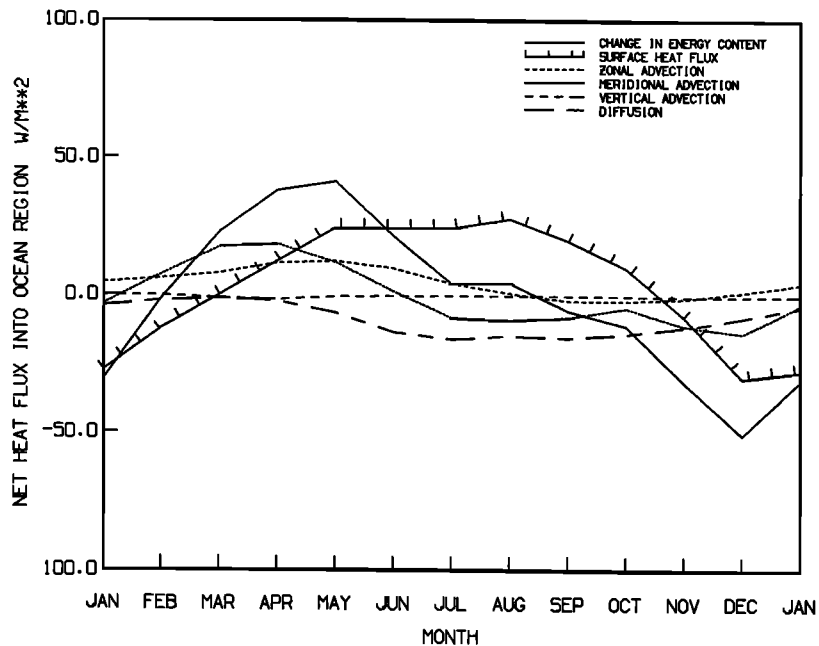


Fig. 16b

Fig. 16. Same as Figure 14 but for the region from 145°W to 115°W and 4°N to 12°N.

bility than is suggested by surface observations (W. B. Rossow, personal communication, 1987). Since the model is too warm where the cloud cover is a maximum and too cold where it is a minimum, these are changes of the sign required to reduce the remaining discrepancies between simulated and observed SST.

Runs using constant cloud cover everywhere and at all times and with monthly cloud cover have demonstrated that although the radiative effect of the annual mean cloud cover distribution has a first-order effect on the SST field, the relatively small seasonal variation of cloud cover is apparently of secondary importance. Confirmation of this will have to wait until more reliable, satellite-derived, cloud data become available. In addition, since only total cloud cover goes into the solar radiation parameterization, details of vertical atmo-

spheric structure are not considered in the determination of model SST.

Experiments with the model have demonstrated the critical role that dynamics plays in determining the SST of certain parts of the tropical Pacific. The full three-dimensional temperature equation is required to model this role. Further away from the equator the heat balance is closely approximated by a balance between the surface heat flux and the change in heat storage. Even though there is a clear seasonal cycle of mixed layer depth at these latitudes, use of a constant depth mixed layer allows a fair representation of the seasonal cycle of temperature. This was due to the strength of the negative feedback between the SST and the surface heat flux. Inclusion of a variable depth mixed layer is one possible addition to the model that should improve its performance.

This project was begun with the goal of calculating the surface heat flux the model requires in order to correctly simulate the SST. By comparing this flux with that observed it was hoped that it would be possible to identify problems in the ocean model: what physics is wrong and what physics is missing. It was soon realized that the heat flux data was not reliable enough to make satisfactory conclusions, and it was decided to adopt the methodology presented here. Thus the SST became the parameter with which to test the model, but we are now faced with the problem that errors in the specified atmospheric variables which go into the model are sufficient to remove the discrepancies. Throughout the paper, where we think ocean dynamics are the cause of problems, it has been pointed out, but beyond that it is not possible to prove model failings. That is not to say that they do not exist. They almost certainly do, but it is required to look at variables other than SST to identify them. A discouraging implication is that SST, the best observed of all oceanic variables, cannot be used as a test of sophisticated ocean GCMs. Only a breakthrough in the ability to specify surface heat flux would change this situation.

The feasibility of modelling the major features of the mean tropical Pacific SST using a simple dynamical model and surface heat flux parameterization has been established. Future work will involve coupling of the ocean model to a model atmosphere in an attempt to simulate the SST and atmospheric phenomena not as independent features, but as different aspects of the same coupled system.

*Acknowledgments.* The comments and criticisms of earlier drafts by many colleagues are gratefully appreciated. Without them this paper would have been completed much earlier. R.S. was supported by NASA co-operative agreement NCC 5-29 with Columbia University. S.E.Z. was supported by National Science Foundation grant NSF-ATM86-12570, and M.A.C. was supported by National Aeronautics and Space Administration grant NASA-NAGW-916. Lamont-Doherty Geological Observatory contribution 4240.

#### REFERENCES

- Blanc, T. V., Accuracy of bulk method determined flux, stability, and sea surface roughness, *J. Geophys. Res.*, **92**, 3867–3876, 1987.
- Cane, M. A., and R. J. Patton, A numerical model for low frequency equatorial dynamics, *J. Phys. Oceanogr.*, **14**, 1853–1863, 1984.
- Esbensen, S. K., and V. Kushnir, The heat budget of the global ocean: An atlas based on estimates from surface marine observations, *Rep.* **29**, 27 pp., 188 figs., Clim. Res. Inst., Oreg. State Univ., Corvallis, 1981.
- Han, Y., A numerical world ocean general circulation model, II, A baroclinic experiment, *Dyn. Atmos. Oceans*, **8**, 141–172, 1984.
- Haney, R. L., Surface thermal boundary condition for ocean circulation models, *J. Phys. Oceanogr.*, **1**, 241–248, 1971.
- Hansen, D. V., and C. A. Paul, Genesis and effects of long waves in the equatorial Pacific, *J. Geophys. Res.*, **89**, 10,431–10,440, 1984.
- Levitus, S., Climatological atlas of the world ocean, *NOAA Prof. Pap.* **13**, 173 pp., 1982.
- Meehl, G. A., and W. M. Washington, Sea surface temperature computed by a simple ocean mixed layer model coupled to an atmosphere GCM, *J. Phys. Oceanogr.*, **15**, 92–104, 1985.
- Meehl, G. A., W. M. Washington, and A. J. Semtner, Experiments with a global ocean model driven by observed atmospheric forcing, *J. Phys. Oceanogr.*, **12**, 301–312, 1982.
- Payne, R. E., Albedo of the sea surface, *J. Atmos. Sci.*, **29**, 959–970, 1972.
- Philander, S. G. H., and R. C. Pacanowski, A model of the seasonal cycle in the tropical Atlantic Ocean, *J. Geophys. Res.*, **91**, 14,192–14,206, 1986a.
- Philander, S. G. H., and R. C. Pacanowski, The mass and heat budget in a model of the tropical Atlantic Ocean, *J. Geophys. Res.*, **91**, 14,212–14,220, 1986b.
- Rasmusson, E. M., and T. H. Carpenter, Variations in tropical sea surface temperature and surface wind fields associated with the Southern Oscillation/El Niño, *Mon. Weather Rev.*, **110**, 354–384, 1982.
- Talley, L. D., Meridional heat transport in the Pacific Ocean, *J. Phys. Oceanogr.*, **14**, 231–241, 1984.
- Weare, B. C., P. T. Strub, and M. D. Samuel, Marine climate atlas of the tropical Pacific Ocean, 147 pp., Dep. of Land, Air, and Water Resour., Univ. of Calif., Davis, 1980.
- Weare, B. C., P. T. Strub, and M. D. Samuel, Annual mean surface heat fluxes in the tropical Pacific Ocean, *J. Phys. Oceanogr.*, **11**, 705–717, 1981.
- Wyrtki, K., An estimate of equatorial upwelling in the Pacific, *J. Phys. Oceanogr.*, **11**, 1205–1214, 1981.
- Zebiak, S. E., A simple atmosphere model of relevance to El Niño, *J. Atmos. Sci.*, **39**, 2017–2027, 1982.
- Zebiak, S. E., Tropical atmosphere-ocean interaction and the El Niño/Southern Oscillation phenomenon, Ph.D. thesis, 261 pp., Mass. Inst. of Technol., Cambridge, 1984.
- Zebiak, S. E., Atmospheric convergence feedback in a simple model for El Niño, *Mon. Weather Rev.*, **114**, 1263–1271, 1986.
- Zebiak, S. E., and M. A. Cane, A model El Niño–Southern Oscillation, *Mon. Weather Rev.*, **115**, 2262–2278, 1987.

M. A. Cane and S. E. Zebiak, Lamont-Doherty Geological Observatory, Palisades, NY 10964.

R. Seager, NASA Goddard Institute for Space Studies, 2880 Broadway, New York, NY 10025.

(Received July 7, 1987;  
accepted August 6, 1987.)